Design of a Compact Dual-band Textile Antenna Based on Metasurface

Kai Zhang, Ping Jack Soh, and Sen Yan

***Abstract*—This paper presents a compact textile antenna design based on a metasurface for wearable applications. It operates in the 2.45 GHz and 5.5 GHz industrial, scientific, and medical bands. A two-dimensional equivalent circuit model is proposed to provide insight into the working principle of the metasurface. The tuning of the radiator's resonant frequencies can be easily performed by adjusting the dispersion curve of the metasurface unit cell. The metasurface in this work consists of a 4×4 array of unit cells fed by a printed coplanar waveguide structure with a slot in its reverse side to maintain its low profile structure. The main innovations of this work are: (i) the -2nd mode is employed to significantly miniaturize the antenna dimensions; (ii) the simultaneous excitation of the +1st mode to enable dual-band operation; (iii) an integrated back reflector to reduce back radiation and lower SAR; and (iv) the use of full textile materials to guarantee user comfort, ease of fabrication and low cost. The proposed antenna's footprint is 44.1 × 44.1 mm² (0.12λ² at 2.45 GHz), with an impedance bandwidth of 10.2 % centered at 2.45 GHz and 22.5 % at 5.5 GHz. The maximum gain is -0.67 dBi and 7.4 dBi in free space, and 9 % of power gain attenuation is generated when used on the body, and is suitable as a miniaturized antenna for wearable applications.**

***Index Terms*—Metasurface, textile antennas, compact antennas, dual-band antennas, circuit model, wireless body area networks.**

I. INTRODUCTION

FLEXIBLE wireless devices have been increasingly important to cater to advanced communication systems in the Internet of Things (IoT) and 5G [1]-[3]. As shown in Fig. 1, these devices are becoming an important element in the Wireless Body Area Network (WBAN) in applications such as health monitoring, medical care, emergency rescue, location services, wireless communication, virtual reality, control and interface to the brain, and etc. For instance, in health monitoring, a contactless detection system has been proposed in [4] to clinically diagnose Parkinson's disease. The use of compact and conformal antennas operating in the C-band are crucial in this detection system. Meanwhile, in [5], a nonintrusive breathing monitoring system using the C-band sensing technique was proposed. The microwave sensing platform developed in this system obtained breathing-induced chest movements in diabetic patients. Its device for signal transmission needs an off-body transmits wearable antenna with broadside radiation and skin-friendly material. Finally, the work in [6] presented a wearable wireless sensing system to assist patients affected by Parkinson's disease. Integrated micro-electro-mechanical inertial sensors are used to recognize incidences of involuntary gait freezing and communicate the data to the signal transmitting unit. Small and comfortable antennas are vital in such devices worn on the human body. An electrically small antenna with a low profile metasurface cloak is presented for medical internet-of-things [7]. This metasurface cloak compensates for the capacitive nature of an electrically small dipole to enable resonance. These antennas' flexibility, low profile, and miniaturization are the essential features in WBAN systems [4]-[10]. Meanwhile, specific absorption rate (SAR) is also another important parameter in determining the safety levels of wearable antennas [11], [12].

Fig. 1. WBAN and its applications.

In recent years, various materials and fabrication techniques have been employed to produce flexible antennas. They include inkjet-printed antennas [13], [14], polyimide film [15] or

Manuscript is submitted on XXX, 2021. This project is supported by the National Natural Science Foundation, China (No. 61901351). P. J. Soh would like to acknowledge the support by the Academy of Finland 6 Genesis Flagship (grant no. 318927). (Corresponding author: S. Yan)

K. Zhang and S. Yan are with the School of Information and Communications Engineering, Xi'an Jiaotong University, Xi'an 710049, China. (e-mail: sen.yan@xjtu.edu.cn). P. J. Soh is with Centre for Wireless Communications, University of Oulu, Oulu, FI-90014, Finland.

Color versions of one or more of the figures in this communication are available online at http://ieeexplore.ieee.org.

Digital Object Identifier xxxx

polydimethylsiloxane (PDMS)-based antennas [16], [17], and silicone-based antennas [18]. Their selection can be made depending on their properties to suit the requirements of different application. Flexible materials for antennas used in clothes are also made using textiles. Felt, leather, denim, silk, etc., are popular due to their comfort and skin-friendliness [19].

In recent years, novel design methods, materials, fabrication technologies, and applications are being developed, spurring the emergence of flexible antennas. One of the key areas being investigated is the application of metamaterials on wearable antennas [20]-[45]. This resulted in novel antennas designed with special radiation characteristics. Examples of metamaterials applied in wearable antenna designs include the composite right/left-handed transmission lines (CRLH TLs) and metasurface. The former can be implemented as zero-order resonant (ZOR) antennas [20], [21] and metamaterial-inspired dual-band antennas [22], [23]. It includes ε-negative (ENG), μ-negative (MNG), and dual-negative (DNG) [24]-[26], in [25], [26], an elliptical patch antenna with MNG metamaterial is proposed. These structures provide wide flexibility in the design and manipulation of its radiation property. On the other hand, metasurfaces can be either be artificial magnetic conductor (AMC) [27]-[30], electromagnetic band-Gap (EBG) [31], [32], high-impedance surface (HIS) [33] and etc. Despite being more easily designed and fabricated, CRLH TL-based antennas are intrinsically narrowband, which then limits their applicability. In contrast, metasurface-based antennas offer relatively wider bandwidths and are more suited for wearable applications.

One of the metamaterial-based structures, AMC planes have been widely used as a reflector in planar antennas, resulting in reasonably low profile wearable antennas [27]-[36]. In [34], [35], dual-band coplanar patch antennas integrated with AMC planes were reported, whereas meta-wearable antennas with and without the metasurface plane were studied in [36] and [37], respectively. Meanwhile, the performance of antennas under deformations such as crumpling was also studied. The different aspects investigated in literature showed the AMC plane's effectiveness in improving wearable antennas' gain, directivity, efficiency, front-to-back ratio, compactness, and SAR [38], [39]. However, a drawback of this method the larger sizes of AMC structures, which may limit their application in space-constrained wearable systems.

To alleviate this, an alternative to metasurface-based antennas has been recently proposed by treating the metamaterial structure itself as the main radiator [40]-[45]. For instance, a compact, fully textile antenna loaded with a metamaterial-inspired structure was presented in [23]. It operates using the -1 and +1 modes of a CRLH-TL to enable dual-band operation. Furthermore, such metasurface antenna can be developed from a one-dimensional CRLH-TL, which reduces its size relative to conventional designs. The operating frequency of this miniaturized antenna can be tuned by controlling its dispersion curves, which was also validated in [43]-[45]. It is worth noting that these antennas are typically designed on rigid materials, which is not suitable for integration with clothings. Moreover, such topology can only be formed using dual-layered substrates, which potentially causes manufacturing errors during fabrication. To some extent, the height of the antenna still needs to be decreased.

In this paper, a fully textile and compact dual-band antenna based on metasurface is proposed for WBAN application. The metasurface functions as the main radiator, which operate using a pair of modes (+1 and -2 modes) based on the CLRH TL theory, resulting in dual band operation. In contrast to the existing use of mode pair solutions in dual-band antennas from [18]-[20], the -2 operating mode introduced on the metasurface in this work resulted in a significant antenna size reduction to $0.36 \times 0.36 \times 0.04\ \lambda^3$ (at 2.45 GHz). This metasurface radiator is fed by a coplanar waveguide (CPW)-based coupling feed to enable a low-profile and simple structure for ease of fabrication. While such coupled feed type reduces back radiation [43], exciting an additional resonance for dual band operation will then again result in additional backward radiation [44]. To alleviate this, the CPW feed section is innovatively modified in this work with a slot to not only enable dual band operation and suppress back radiation, but also to reduce the radiator's thickness. Finally, a flexible reflector plane is integrated on the reverse side of the antenna.

The proposed antenna is made fully using flexible textile materials using two felt substrate layers and conductive fabric as the conductive elements. This provides a conformal planar structure which is easily integrated onto clothings for medical applications. Most importantly, the feed, radiator and reflector structure are all optimized jointly to significantly reduce SAR level, ensuring a safe long-term operation of the antenna on the human body. To further simplify the understanding of the operating mechanism, an equivalent circuit model of the metasurface is modeled and analyzed. Finally, the prototyped and measured antenna is validated to operate in the lower band from 2.25 GHz to 2.5 GHz and in the upper band from 5.21 GHz to 6.45 GHz.

The structure of this paper is as follows. In the next section, the antenna design is presented, with an emphasis on the metasurface design principles and processes. Next, the fabricated prototype is measured, its results presented and discussed in Section III. Section IV evaluates the antenna's performance on the human body to verify its applicability for WBAN application. Finally, concluding remarks from this work are presented in Section V.

II. ANTENNA DESIGN AND PRINCIPLES

A. Metasurface design

The metasurface plane is an important component of the proposed antenna. In contrast to a transmission line which can generate resonance, the metasurface plane not only can generate positive resonances but also negative resonances due to its intrinsic properties. These resonances can be identified via dispersion relation, which are then used to calculate resonant frequency in different modes. To design these planes, the dispersion property of its unit cell needs to be first calculated, based on the validated procedures in [40]-[45]. In this work, the unit cell is first designed and centered on a

This article has been accepted for publication in a future issue of this journal, but has not been fully edited. Content may change prior to final publication. Citation information: DOI 10.1109/TBCAS.2022.3151243, IEEE Transactions on Biomedical Circuits and Systems

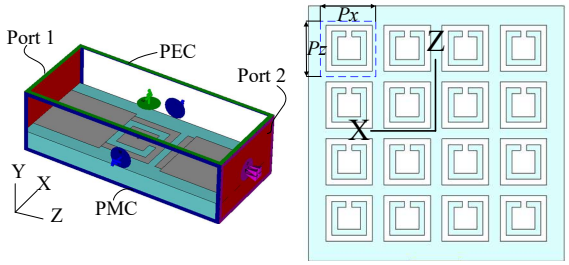

(a) (b)

Fig. 2. (a) Modeled unit cell for dispersion simulations, and (b) metasurface plane.

transmission line, and its boundary condition is setup as in Fig. 2(a). The unit cell is then excited by the two ports to generate the quasi TEM mode. This indicates that the phase delay in the *x*-direction is 0°. The dispersion of the unit cell in the *z*-direction can then be calculated based on the S parameters, as follows [46],

$$P_{x(z)} = \beta_{x(z)} \times px(z) = \cos^{-1}\left(\frac{1 - S_{11}S_{22} + S_{12}S_{21}}{2S_{21}}\right) \quad (1)$$

in (1), $P_{x(z)}$ is the phase delay of the unit cell in the $x(z)$-direction, $px(z)$ is the length of the unit cell in different directions (as shown in Fig. 2(b)), and $\beta_{x(z)}$ is the propagation constant. The metasurface plane consists of a 4 ×4 metasurface unit cell array. Based on the resonant condition [43],

$$P_{x(z)} \times N_{x(z)} = n(m)\pi \ , \ n(m) = 0, \ \pm 1, \ \pm 2, \ \cdots \quad (2)$$

where $N_{x(z)} = 4$ is the number of the unit cell in a metasurface plane. From [43], it is observed that the footprint of the metasurface antenna operating using -1 mode lacks compactness due to the low permittivity of the felt substrate. Thus, -2 mode is chosen instead in this work, which further miniaturizes the proposed antenna while maintaining its flexibility. To enable dual-band operation in this work, the following two resonant modes are chosen: -2 mode at 2.5 GHz and +1 mode at 5.5 GHz. Dimensions of the metasurface unit cell are then optimized to obtain the resonant frequencies, resulting in the final dispersion curve shown in Fig. 3 (solid black line).

B. Working mechanism and equivalent circuit model

The aforementioned metasurface design method is analyzed from the simulation model's perspective. For a more comprehensive insight into its working mechanism, a two-dimensional equivalent circuit model is proposed for the metasurface plane, as illustrated in Fig. 4(a) [47], [48]. This circuit model is also more sophisticated, as it considers circuit parameters in the orthogonal directions. Several other works have also studied the impedance of metasurfaces and built explicit expressions from the electromagnetic field theory [49]-[51]. Analysis of the spatial distributions of vector fields and electromagnetic energy presented in these works can be used to better estimate the metasurface performance assuming infinite electromagnetic properties in three-dimensional space. On the other hand, in this paper, the circuit theory is used to obtain the surface impedance of the metasurface, which relates the electromagnetic law in two-dimensional space. Nonetheless,

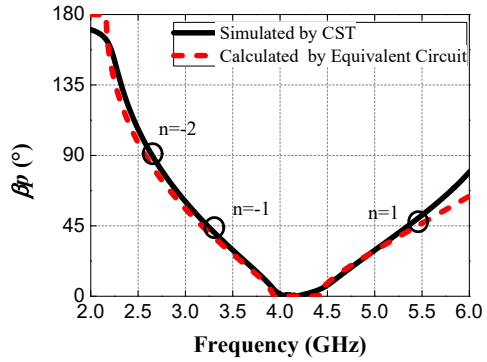

Fig. 3. Dispersion curves simulated in CST and calculated using the proposed equivalent circuit when P_x=0°.

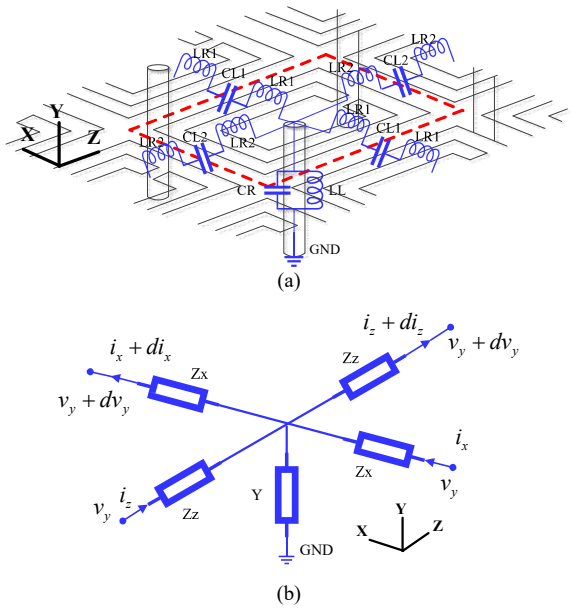

Fig. 4. (a) Unit cell of the metasurface, and (b) its equivalent circuit model.

both methods are related and can be understood by engineers depending on their preference. The gaps between two-unit cells are modeled as series capacitances C_{L1} and C_{L2}. Each unit cell is connected to the substrate by using a flexible metal wire, which is then modeled as a parallel inductance L_L. Meanwhile, a parallel capacitance, C_R is generated between the radiator and the ground. The series inductances L_{R1} and L_{R2} originates from the radiator itself, and the U-shaped slot increases their level further. Nonetheless, this complex circuit model can be further simplified as shown in Fig. 4(b). Combining these two circuit models, (3)-(5) then can be deduced as [47],

$$Z_x(\omega) = \frac{1}{2j\omega C_{L1}} + j\omega L_{R1} \quad (3)$$

$$Z_z(\omega) = \frac{1}{2j\omega C_{L2}} + j\omega L_{R2} \quad (4)$$

$$Y(\omega) = \frac{1}{j\omega L_L} + j\omega C_R \quad (5)$$

This article has been accepted for publication in a future issue of this journal, but has not been fully edited. Content may change prior to final publication. Citation information: DOI 10.1109/TBCAS.2022.3151243, IEEE Transactions on Biomedical Circuits and Systems

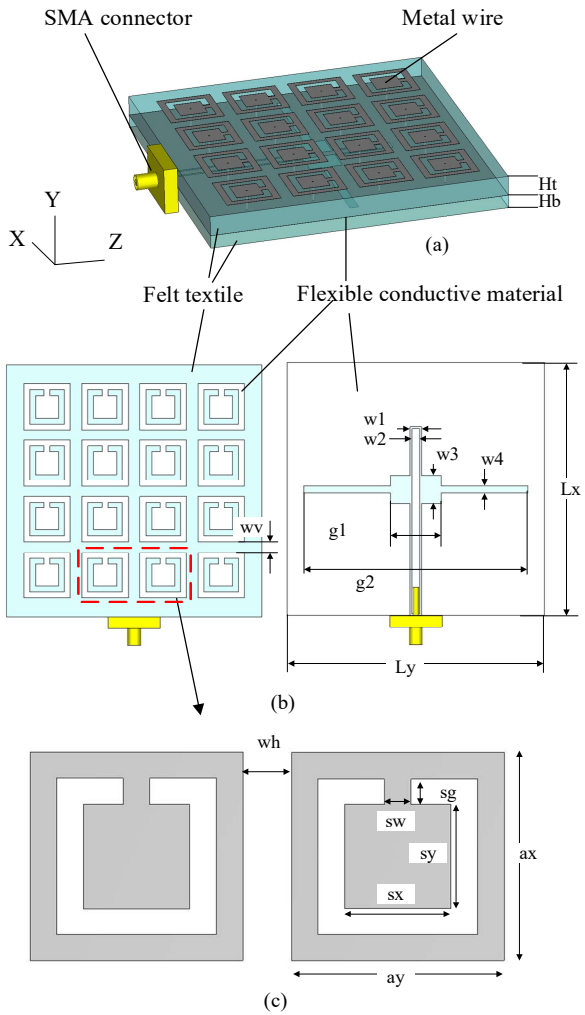

Fig. 5. The geometry of the proposed flexible antenna, (a) dimensions of antenna, (b) the top view and the back view, (c) dimensions of metasurface unit cell.

TABLE I
DIMENSIONS OF THE ANTENNA 1 OF FIG. 5

Parameter	Value (mm)	Parameter	Value (mm)
Ht	*3.0*	*g2*	*38.3*
Hb	*2.0*	*ax*	*8.0*
Lx	*44.1*	*ay*	*8.0*
Ly	*44.1*	*wh*	*2.0*
w1	*2.0*	*wv*	*1.8*
w2	*1.3*	*sg*	*1.0*
w3	*4.8*	*sw*	*1.0*
w4	*1.3*	*sx*	*4.0*
g1	*9.1*	*sy*	*4.0*

From the equivalent model in Fig. 4(b), the following relations are obtained,

$$\partial v_y/\partial x = -i_x \cdot 2Z_x \quad (6)$$

$$\partial v_y/\partial z = -i_z \cdot 2Z_z \quad (7)$$

$$\partial i_x/\partial x + \partial i_z/\partial z = -v_y Y \quad (8)$$

Based on (6) to (8), equations (9) and (10) are then obtained when only one direction of phase delay is considered.

$$\partial^2 v_y/\partial x^2 + \beta_x^2 v_y = 0,\ \beta_x = \sqrt{-2Z_x Y}\ \ (Pz{=}0) \quad (9)$$

$$\partial^2 v_y/\partial z^2 + \beta_z^2 v_y = 0,\ \beta_z = \sqrt{-2Z_z Y}\ \ (Px{=}0) \quad (10)$$

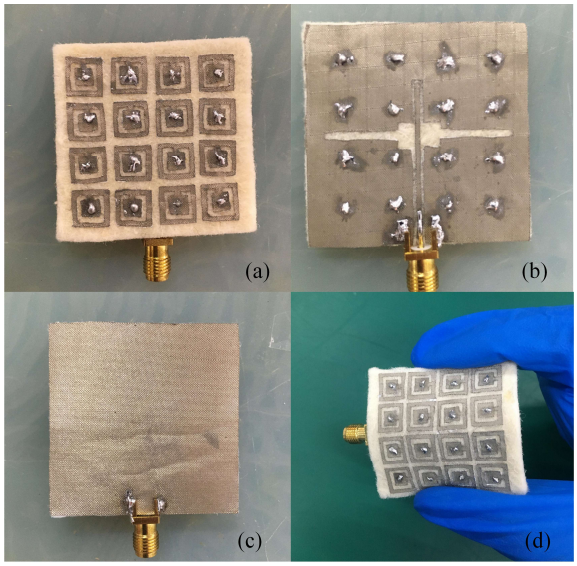

Fig. 6. Prototype of the flexible antenna. (a) top view, (b) feeding structure, (c) back view, and (d) its flexibility.

The equivalent length of the circuit model of a unit cell in this paper is the physical length of the unit cell, $px(z)$, with the phase delay in the x-direction set as 0°. Thus from (4), (5) and (10), the dispersion is expressed as:

$$\beta(\omega)pz = \sqrt{2\omega^2 L_{R2}C_R + \frac{1}{\omega^2 L_L C_{L2}} - \left(\frac{2L_{R2}}{L_L} + \frac{C_R}{C_{L2}}\right)} \quad (11)$$

Using equations (2) and (11), and according to Taylor expansion of the cosine function, the circuit parameters can then be expressed as follows,

$$\frac{n(m)\pi}{N_{x(z)}} = \cos^{-1}\left(1 - \frac{1}{2}\left(2\omega^2 L_{R2}C_R + \frac{1}{\omega^2 L_L C_{L2}} - \left(\frac{2L_{R2}}{L_L} + \frac{C_R}{C_{L2}}\right)\right)\right) \quad (12)$$

From (12), the fitted circuit parameters are obtained, as follows: C_{L2}=0.65 pF, C_R=1.5 pF, L_L=1.1 nH, and L_{R2}=1.0 nH. Meanwhile, the corresponding dispersion curve is plotted in Fig. 3 and compared to CST simulation results. It also shows that the proposed unit cell introduces a 90° phase delay at about 2.45 GHz in the left-hand band, and a 45° phase delay at about 5.5 GHz in the right-hand band. They represent the -2 and +1 resonant modes, respectively.

C. Antenna design guideline

Based on the aforementioned principles, an antenna with an overall dimension of 44.1 ×44.1 × 5 mm^3 (0.36 × 0.36 × 0.04 λ^3 at 2.45 GHz) is designed, as shown in Fig. 5(a). It consists of a CPW feeding structure and a metasurface plane located on the two sides of the same textile substrate, as illustrated in Fig. 5(b). The slot feeding structure is chosen to excite an anti-phase mode of the antenna [42]. Different from other designs in literature [52], [53], the CPW feeding structure is integrated into the ground of the antenna in this design, which avoided the need for a separate strip feeding structure and decreased the profile. This then also simplifies the fabrication process using textiles. As an alternative, the stepped feeding slot is used to

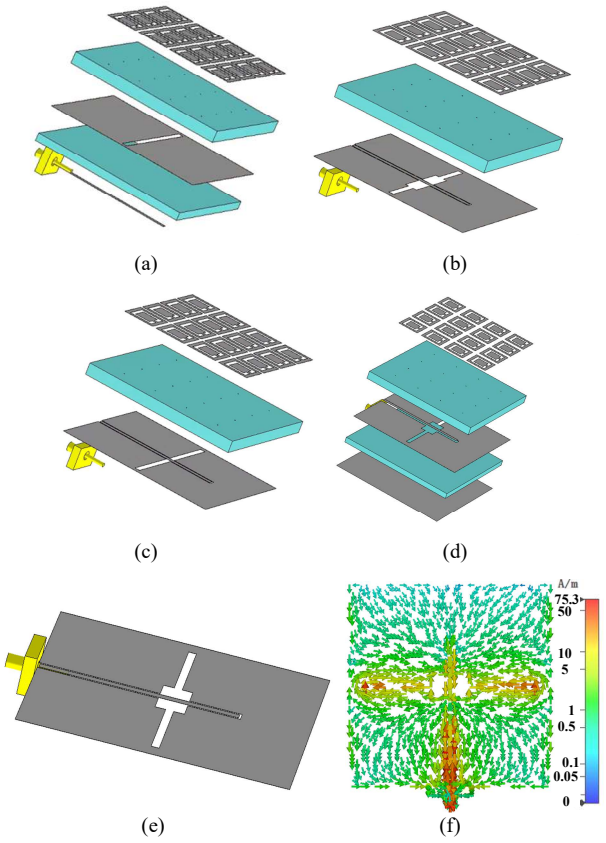

Fig. 7. Evolution of the flexible antenna. (a) case 1, (b) case 2, (c) case 3, (d) the proposed antenna, (e) CPW antenna (f) the current distribution of the CPW antenna at 4.2 GHz.

improve impedance matching. The feeding and radiating structures are made using ShieldIt Super® conductive textiles, with a conductivity of 1.18×10^5 S/m and 0.017 mm of thickness. The substrate chosen is felt, with 3 mm thickness, and relative permittivity (εr) and loss tangent ($tan\delta$) of 1.3 and 0.044, respectively. All the parameters of the proposed antenna are listed in Table I.

Next, the fabricated prototype of the flexible antenna is shown in Fig. 6. Two layers of felt with different thicknesses (3 mm and 2 mm) are used in this design. The 4 ×4 metasurface unit cell array made of conductive textiles is secured onto the top face of the 3 mm thick felt substrate with glue, whereas the CPW feeding structure is placed in between the two substrates. On the other hand, copper wires with 0.8 mm diameter are inserted through the textiles to connect the metasurface unit cells and the ground of the CPW feeding structure. To ensure consistent galvanic connection, both ends of the copper wires are soldered onto the conductive textile. Finally, the bottom side of the last layer is fully covered using the conductive textile. An SMA connector is soldered directly at the end of feed line, as shown in Fig. 6(b). The welding temperature should not exceed 260 ℃ to avoid disintegration of the conductive fabric. Prior to its full evaluation, the antenna performance is also repeatedly measured to ensure that it is stable.

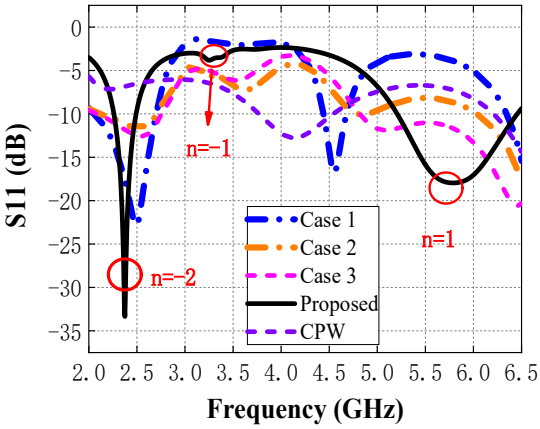

Fig. 8. S_{11} of the flexible antenna.

To ensure fabrication robustness, it is noted that the optimized dimensions from simulations will need to be traded off with realistic fabrication accuracy using manual tools. The two main dimensions which needed to be compromised include the diameter of the shorting vias and 0.3-mm gap between the CPW line and ground plane. To find the best dimension for them, parametric studies are conducted, with a 0.5 mm lowest accuracy. It is found that the antenna is still able to operate throughout the target frequency bands while maintaining performance robustness, even when slight changes may occur on these parameters during the fabrication process.

In the design process, the antenna is optimized in four main steps (denoted as "cases") shown in Fig. 7(a)-(d), with their reflection coefficient (S_{11}) curves shown in Fig. 8. The structure in Case 1 is designed from a typical metasurface antenna. Despite having a compact size, this antenna requires an additional substrate layer for the feeding structure, besides being limited in bandwidth in the higher frequency band. Integrating a CPW structure resulted in the structure shown in Case 2, which featured a wider bandwidth in the higher frequency band. Next, a stepped slot is used in place of a regular slot to facilitate impedance matching in Case 3. This resulted in improved S_{11}, but then produced additional back radiation, which potentially increases SAR. To alleviate this, a reflector is then designed and located on the back of the antenna. The final proposed antenna is shown in Fig. 7(d).

To study the influence of the CPW structure on the metasurface plane, the current distribution of the CPW line and its S_{11} are presented in Fig. 8. It is observed that the current shows a slot radiation mode, which slot length is about half of a wavelength at 4.2 GHz. It validates that the +1 mode of metasurface antenna is not excited by the CPW structure. Moreover, the input impedance of the CPW structure is not 50 Ω, and it is matched using the stepped structure of the slot. There are two main reasons for not directly designing a 50 Ω CPW structure: i) to maintain structural simplicity, and ii) to maintain design simplicity. For the former, either the width of the feed line is too long or the gap between the feed line and ground is too small to enable a 50 Ω CPW impedance. These configurations will further complicate the antenna fabrication

This article has been accepted for publication in a future issue of this journal, but has not been fully edited. Content may change prior to final publication. Citation information: DOI 10.1109/TBCAS.2022.3151243, IEEE Transactions on Biomedical Circuits and Systems

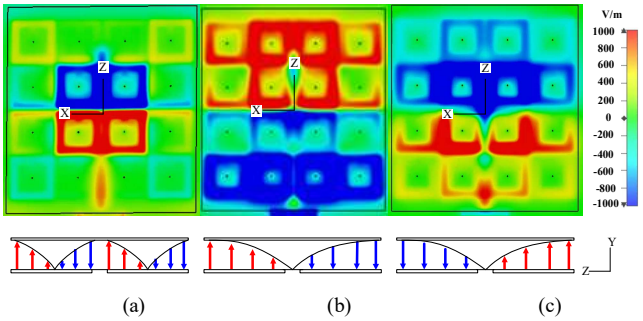

Fig. 9. The amplitude of E-field along the *y*-direction (a) -2 mode at 2.45 GHz, (b) -1 mode at 3.3 GHz and (c) +1 mode at 5.5 GHz.

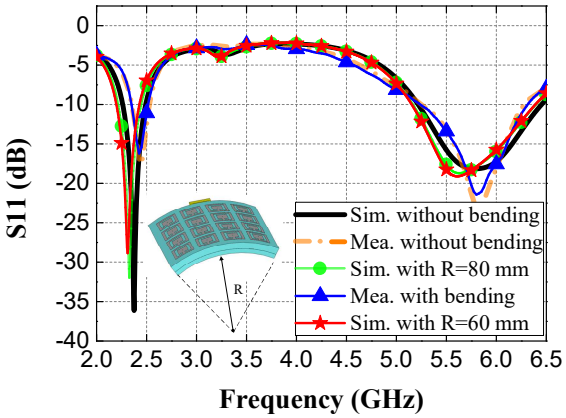

Fig. 10. S_{11} curves of the flexible antenna with different states.

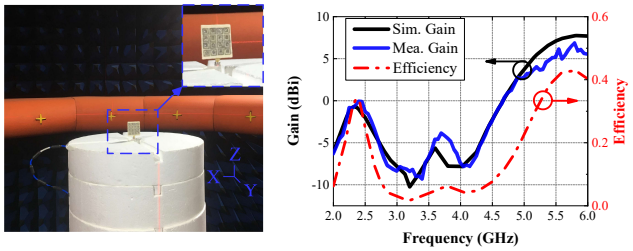

Fig. 11. (a) Antenna measurement setup in an anechoic chamber, (b) gain and efficiency over the working band.

process. For the latter, the feeding structure and metasurface plane are optimized as a single system to simplify the design procedure. The feeding structure is designed with a 50 Ω input impedance to match the SMA connector's impedance, and the rest of the CPW structure acts as an impedance transformer between the connector and metasurface plan.

In addition to the S_{11}, the distribution of the electric field's *y*-component (vertical component) is shown in Fig. 9. When excited by a slot feeding structure, the E-field distribution at 2.45 GHz is an anti-phase TM(-20) mode, and another at 5.5 GHz is a TM(10) mode. Besides that, the TM(-10) mode at 3.3 GHz is also presented in Fig. 9 (b). The E-field distribution shows that the +1 mode and -1 modes are anti-phase, with the -2 mode is also anti-phase due to the slot feeding, which can excite broadside radiation. The E-field vector in the *yz* plane presented in Fig. 9 agreed with the dispersion curve modes.

As a summary, the antenna design can be performed as follows.

1) Metasurface design

An appropriate metasurface unit is designed to includea parallel resonant tank and a series resonant tank to generate left-hand characteristic. Then, a transmission dispersion simulation is modeled as shown in Fig. 2(a) and applying the dispersion calculation formula (1) in the post-processing module in CST. The structure of the metasurface unit is then optimized to adjust the corresponding modes in the dispersion curve to the designed frequencies.

2) Feeding structure design

Coupled feeding techniques are widely used in metasurface plane excitation [40]-[44]. To excite the -2 mode, the gap coupling feeding technique with CPW structure is employed, decreasing the antenna's thickness relative to conventional coupled feeding techniques.

3) Optimizing front-to-back ratio

Due to the compact size of the proposed antenna, a monopole-like radiation mode is excited. This is unsuitable for WBAN applications. Thus, a reflection plane is designed and integrated onto the rear of the antenna to effectively decrease this back radiation. Finally, the parameters of the feeding structure is then fine-tuned for optimized performance.

III. Antenna Measurements And Performance

One of the most important properties of textile antennas is being flexible and conformal. For this, the antenna's simulated and measured S_{11} are investigated with bending curvatures of R=60 mm, and R=80 mm, and compared against its planar form (without bending, $R=\infty$), as shown in Fig. 10. An Agilent AV3672E-S vector network analyzer (VNA) is used for measurements. In planar form, the simulated bandwidth is from 2.25 GHz to 2.5 GHz (250 MHz, 10.2%) in the lower band and from 5.21 GHz to 6.45 GHz (1240 MHz, 22.5%) in the upper band. On the other hand, measurements indicated a bandwidth from 2.35 GHz to 2.55 GHz (200 MHz, 8.2%) in the lower band and from 5.22 GHz to 6.3 GHz (1080 MHz, 19.6%) in the upper frequency band. It is seen that the simulated S_{11} with $R=\infty$ and R = 80 mm are similar, in agreement with measurements. In the lower band, bending with R = 60 mm is slightly shifted the operating band upwards due to the distortion of the antenna structure. However, the antenna's operation remains unaffected, as it still covers the intended WBAN band. In general, all measurements indicated a slight shift of operation downwards, which is due to the inhomogeneous thickness and permittivity of the textile substrate. Moreover, these observations are also caused by minor fabrication errors caused by the manual procedure and tools. Despite that, it can be seen that generally, measurement results agreed reasonably with simulations.

Next, the antenna's far-field performance is measured in an anechoic chamber, as shown in Fig. 11(a), with its gain and efficiency shown in Fig. 11(b). From simulations, the gain in the lower band is c.a. -0.67 dBi, and in the upper band is c.a. 7.4 dBi. The measured gains are -0.09 dBi and 6.5 dBi, respectively. The simulated efficiency is 34% at 2.45 GHz and 42% at 5.5

This article has been accepted for publication in a future issue of this journal, but has not been fully edited. Content may change prior to final publication. Citation information: DOI 10.1109/TBCAS.2022.3151243, IEEE Transactions on Biomedical Circuits and Systems

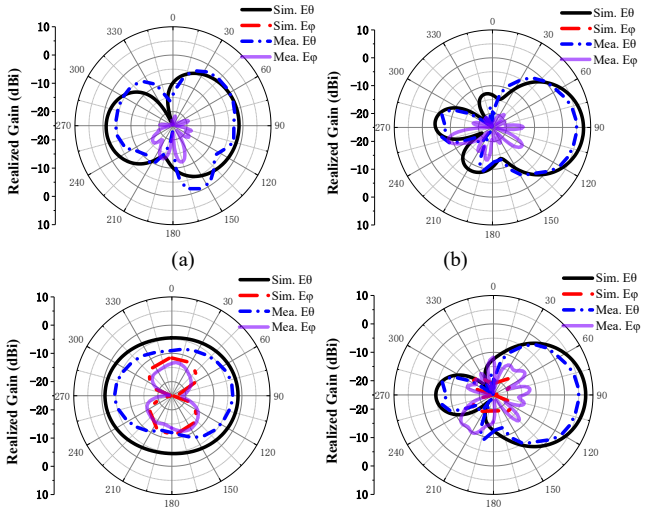

Fig. 12. Far-field patterns of the antenna. (a) *yz* plane at 2.45 GHz, (b) *yz* plane at 5.5 GHz, (c) *xy* plane at 2.45 GHz, (d) *xy* plane at 5.5 GHz. The simulated *Eφ* in (a), (b) and (c) are less than -30 dB.

GHz. The relatively lower efficiency is mainly due to the loss of the substrate layers. Loss of the substrate textile, conductivity of the conductive textile, and antenna dimensions are the main factors limiting efficiency. In this work, replacing the existing substrate with a less lossy one and a more conductive textile can improve the radiation efficiency dramatically. Besides the use of better materials, generation of a uniform current throughout the antenna structure by adjusting the overall antenna can also be considered to enhance its efficiency in future works [54].

The measured far-field patterns are shown in Fig. 12. The lower front-to-back ratio of the antenna, especially in the lower band, is due to the miniaturized antenna beside the leaky feeding slot. However, this is improved when the antenna is placed onto a larger conductive ground. Detailed results are listed in Table II.

IV. Antenna Performance on Human Body

In this section, the performance of the textile antenna on the human body is evaluated, and its flexibility is studied.

A. Antenna performance with different curvatures

As shown in Fig. 14, the textile antenna located on a cubic human body is simulated and measured. The human tissue model consists of four layers: a 2 mm-thick skin layer, a 5 mm-thick fat layer, a 20 mm-thick muscle layer, and a 13 mm-thick bone layer with an area of 150×150 mm^2 [33]. All tissue parameters are obtained from the CST material library. Compared with the whole body model, this tissue model allows shorter simulation time, and is sized at a distance of at least a quarter wavelength between the side of the antenna to ensure validity of results. The gap between the antenna and the human tissues is 10 mm. Moreover, the integrated back reflector minimizes coupling and reflection of energy from the radiator to the body. The voxel model in our simulation has enough accuracy for SAR calculation of general wearable antennas

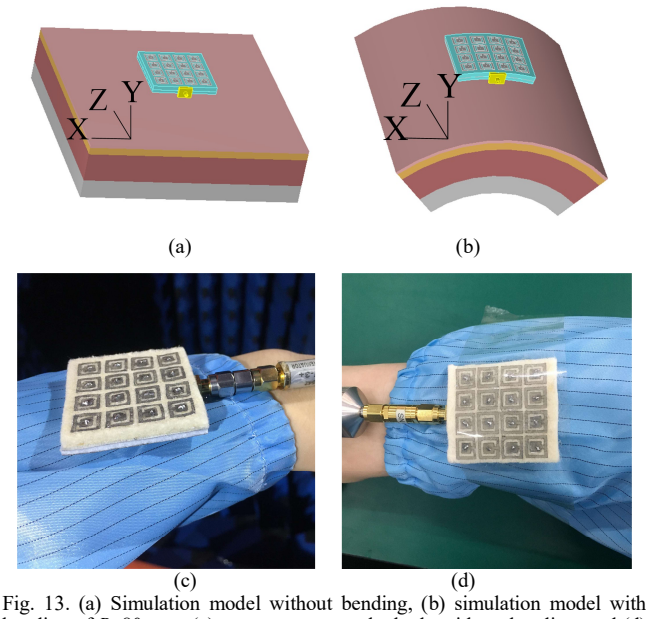

Fig. 13. (a) Simulation model without bending, (b) simulation model with bending of *R*=80 mm. (c) measurement on the body without bending, and (d) measurement on the body with bending.

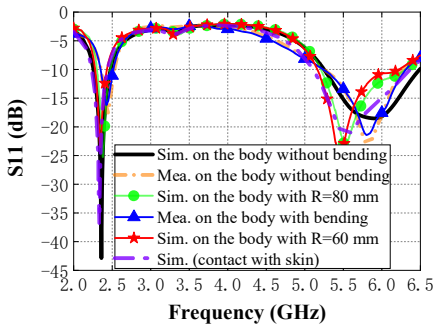

Fig. 14. Simulated and measured the S_{11} when the antenna is bent on the human body.

[55]. The S_{11} of the antenna when placed on the body with different curvatures is studied, and its results are presented in Fig. 14. The prototype sample is placed on the arm with and without bending during measurements to mimic the simulations, as seen in Fig. 13(c) and (d). Results presented in Fig. 14 generally conclude that the antenna's performance is similar when operated on body and bent. Simulations indicated an operation from 2.25 GHz to 2.51 GHz, with 260 MHz (9.4%) of bandwidth in the lower band, and from 5.24 GHz to 6.49 GHz with 1250 MHz (22.7%) of bandwidth in the upper band. Experimental evaluations validated that the antenna operated from 2.35 GHz to 2.55 GHz (200MHz, 8.2%) and 5.22 GHz to 6.3 GHz (1080 MHz, 19.6%), in the lower and upper band, respectively. Meanwhile, on body measurements performed indicated similar S_{11} as in free space. This indicates that the reflector minimized the coupling to the human body. In addition to that, an additional simulation to evaluate the antenna performance when placed directly on the human body is performed. It is evident that the changes in S_{11} when operated at this distance remained almost unchanged. The operation of the antenna on the body in bent configuration is observed to

This article has been accepted for publication in a future issue of this journal, but has not been fully edited. Content may change prior to final publication. Citation information: DOI 10.1109/TBCAS.2022.3151243, IEEE Transactions on Biomedical Circuits and Systems

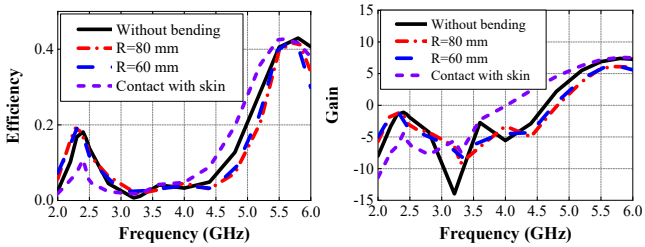

Fig. 15. Simulated gain and efficiency evaluated on the human body.

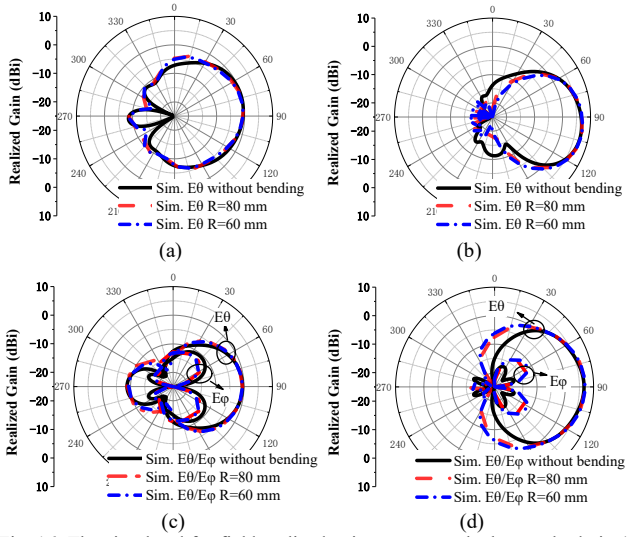

Fig. 16. The simulated far-field realized gain pattern on the human body in (a) yoz plane at 2.45 GHz, (b) yoz plane at 5.5 GHz, (c) xoy plane at 2.45 GHz, (d) xoy plane at 5.5 GHz. The simulated *Eφ* in (a), (b) and (c) are less than -30 dB.

TABLE II
MAIN PERFORMANCE PARAMETERS OF ANTENNAS

Freq. (GHz)	Condition	BW (MHz)	Effi.	Gain (dBi)	SAR (W/kg)
2.45	Sim. in space	250	0.34	-0.67	-
	Mea. in space	200	-	-0.09	-
	Sim. on body	260	0.182	-1.11	0.476
	Mea. on body	200	-	-	-
5.5	Sim. in space	1240	0.42	7.4	-
	Mea. in space	1080	-	6.5	-
	Sim. on body	1250	0.40	7.0	0.024
	Mea. on body	1080	-	-	-

deviate more in the upper band. This is because of the dielectric loading of the human tissue onto the antenna, which also acts as an equivalent substrate and changes the overall effective dielectric constant. Meanwhile, the equivalent wavelength of the upper band is smaller than the lower band, and the bending human tissue has a greater relative curvature. Thus, the higher band experienced more deviation compared to the lower band. Nonetheless, the deviations observed are acceptable, maintaining operating within the target frequency bands.

B. Far-field performance on body

Next, the realized gain and efficiency for this antenna are evaluated, and their results are shown in Fig. 15. Simulations results at 2.45 and 5.5 GHz are -1.11 dBi and 7.0 dBi (in the lower and upper band, respectively), whereas the efficiency is 18.2% and 40.5%. This indicates the significance of the human tissue on the far-field performance. Part of the radiation is absorbed by the body, leading to lower efficiency. Meanwhile, the antenna is further simulated with 0mm distance between the antenna and skin. The efficiency and gain are decreased in the lower band. However, its performance in the upper band is improved compared to the its operation with a 10 mm gap. This is due to the tissue surface which now also reflects the radiated energy from the antenna. Moreover, the higher front-to-back ratio in this band also validates this observation. The radiation patterns of the textile antenna on the human body are illustrated in Fig. 16. The simulation results indicated that the antenna featured a good robustness in performance despite being simulated under different curvatures.

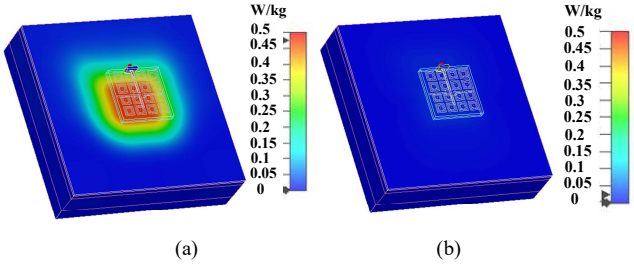

Fig. 17. Simulated SAR of the antenna on the human body with a 10 mm gap at (a) 2.45 GHz and (b) 5.5 GHz.

C. SAR evaluation

When attached to or used near human tissues, a major concern of WBAN antennas is the absorption of their radiation in the human body. This is characterized by the Specific Absorption Rate (SAR), which indicates the tissues' exposure to RF energy from wireless devices. This is regulated at a limit of 2 W/kg, as averaged over ten grams of tissue (IEEE C95.1-2005). To assess this, the antenna is simulated when placed over the human tissue in planar condition. Results in Fig. 17 indicate a peak SAR of 0.476 W/kg at 2.45 GHz and 0.024 W/kg at 5.5 GHz when fed by an input power of 0.2 W. The intended application of the antenna (and the fully covered reverse side) is not to be integrated directly onto the skin of the human user, but rather to be integrated in the coats, which have at least 5 to 10 mm distance from the body using a non-conductive spacer or the clothing itself. In this way, wearable devices can be protected from being affected by the human tissue in their proximity, while avoiding performance variations during operation. So there are no biocompatibility issues in the proposed applications. On the other hand, this conductive plane also reduces the human body from radiation exposure. Even the antenna is located very close to the skin, the SAR values are 0.556 W/kg and 0.051 W/kg, which are well below the exposure limits.

Finally, the performance of the proposed antenna and other state-of-the-art metamaterial-based wearable antennas from the literature are compared in Table III. It can be observed that the proposed antenna provided an improved bandwidth and gain compared to most of the dual-band antennas of the same design concept. Besides that, this antenna also allowed a miniaturized footprint relative to most of the WBAN antennas in literature. Despite its size and the more lossy substrate used which

TABLE III
PERFORMANCE COMPARISON OF THE PROPOSED ANTENNA WITH METAMATERIAL-BASED WBAN ANTENNAS IN LITERATURE

Ref.	Freq.(GHz)	BW(%)	Gain(dB)	Efficiency (free space/ on body)	SAR (W/kg)	Footprint (λ^3)	Substrate (ε_r)
[23]	2.45 5.2	5.5 10.6	-3.5 6.6	0.17(ob) 0.75(ob)	0.37 0.69	0.40× 0.40 × 0.049 (@2.45GHz)	Textile (1.3)
[27]	1.8 2.45	10.9 5.1	1~2	-	0.048	0.90 × 0.90 × 0.012 (@1.8GHz)	Jean. Fabric (1.7)
[34]	2.4	4	6.4	-	0.58	0.71× 0.66 × 0.024	Substrate (3)
[36]	2.45 5.8	4 12	6.4 7.6	-	0.08	0.98× 0.98 × 0.027 (@2.45GHz)	Textile (1.38)
[38]	1.575 2.45	7.6 5.5	1.98 1.94	0.73(ob) 0.86(ob)	0.78 0.71	0.45× 0.45 × 0.029 (@1.575GHz)	Kevlar (1.66)
[39]	2.45 5.5	12 16.3	2.5 0~4	0.4(fs) 0.4(fs)	0.019 0.009	0.82× 0.82 × 0.024 (@2.45GHz)	Textile (1.3)
[43]	2.45	15.7	4.25	0.97(fs), 0.53(ob)	0.65	0.45× 0.43 × 0.036 (@2.45GHz)	Substrate (2.65)
This work	**2.45** **5.5**	**10.2** **22.5**	**-0.69** **7.4**	**0.34(fs), 0.18(ob)** **0.42(fs), 0.40(ob)**	**0.476** **0.024**	**0.36 × 0.36 × 0.04 (@2.45GHz)**	**Felt (1.3)**

affected its efficiency and gain, this design is still a predominant index than [23]. These properties make the antenna suitable for WBAN applications.

V. CONCLUSION

In this paper, a flexible textile antenna is designed based on a compact metasurface. A two-dimensional equivalent circuit model of the metasurface is modeled, and the circuit model parameters are used to analyze the dispersion relation. The -2 mode and the +1 mode are designed to operate the antenna at 2.45 GHz and 5.5 GHz in the ISM and WBAN bands. A unique CPW feeding structure is employed to reduce the profile further. A detailed design procedure is also explained to enable the miniaturization of the antenna, which resulted in a dimension of 44.1 ×44.1 × 5 mm^3 (0.36 × 0.36 × 0.04 λ^3 at 2.45 GHz). The main uniqueness of this design are as follows. The wearable antenna operates using the -2 mode using the metasurface radiator to effectively decrease its dimensions, in comparison to literature. Meanwhile, the +1 mode is also adopted to enable wide dual-band characteristic, with refinement of the feeding structure for ease of integration. A back reflector is introduced to ensure low SAR levels in both bands. The use of the textile materials enabled flexibility, fabrication simplicity and cost effectiveness. When evaluated on body in planar and curved configurations, the proposed antenna indicated a robust operation. These characteristics make it very attractive and suitable for integration into clothing for the health monitoring systems.

REFERENCES

[1] B. Zhao, J. Mao, J. Zhao, H. Yang and Y. Lian, "The Role and Challenges of Body Channel Communication in Wearable Flexible Electronics," *IEEE Trans. Biomed. Circuits Syst.*, vol. 14, no. 2, pp. 283-296, April 2020.

[2] D. Patron et al., "On the Use of Knitted Antennas and Inductively Coupled RFID Tags for Wearable Applications," *IEEE Trans. Biomed. Circuits Syst.*, vol. 10, no. 6, pp. 1047-1057, Dec. 2016.

[3] A. S. M. Alqadami, K. S. Bialkowski, A. T. Mobashsher and A. M. Abbosh, "Wearable Electromagnetic Head Imaging System Using Flexible Wideband Antenna Array Based on Polymer Technology for Brain Stroke Diagnosis," *IEEE Trans. Biomed. Circuits Syst.*, vol. 13, no. 1, pp. 124-134, Feb. 2019.

[4] X. Yang et al., "Contactless Finger Tapping Detection at C-Band," *IEEE Sensors J.,* vol. 21, no. 4, pp. 5249-5258, 15 Feb.15, 2021.

[5] X. Yang, D. Fan, A. Ren, N. Zhao and M. Alam, "5G-Based User-Centric Sensing at C-Band," *IEEE Trans. Ind. Informat.*, vol. 15, no. 5, pp. 3040-3047, May 2019.

[6] A. Kita, P. Lorenzi, R. Rao and F. Irrera, "Reliable and Robust Detection of Freezing of Gait Episodes With Wearable Electronic Devices," *IEEE Sensors J.*, vol. 17, no. 6, pp. 1899-1908, 15 March15, 2017.

[7] P. Y. Chen, H. Huang, and C. H. Hung, "Compact metamaterial-enclosed wireless sensors with subtle perception of internal physical events," *Appl. Phys. Lett.*, vol. 107, no. 19, Nov 9 2015.

[8] S. Yan and G. A. E. Vandenbosch, "Design of Wideband Button Antenna Based on Characteristic Mode Theory," *IEEE Trans. Biomed. Circuits Syst.*, vol. 12, no. 6, pp. 1383-1391, Dec. 2018.

[9] F. Kong, M. Zada, H. Yoo and M. Ghovanloo, "Adaptive Matching Transmitter With Dual-Band Antenna for Intraoral Tongue Drive System," *IEEE Trans. Biomed. Circuits Syst.*, vol. 12, no. 6, pp. 1279-1288, Dec. 2018.

[10] J. Zhang, S. Yan, X. Hu and G. A. E. Vandenbosch, "Dual-Band Dual-Polarized Wearable Button Array With Miniaturized Radiator," *IEEE Trans. Biomed. Circuits Syst.*, vol. 13, no. 6, pp. 1583-1592, Dec. 2019.

[11] K. Zhang, P. J. Soh, and S. Yan, "Meta-Wearable Antennas—A Review of Metamaterial Based Antennas in Wireless Body Area Networks," *Materials*, vol. 14, no. 1, p. 149, Dec. 2021.

[12] A. S. M. Alqadami, K. S. Bialkowski, A. T. Mobashsher and A. M. Abbosh, "Wearable Electromagnetic Head Imaging System Using Flexible Wideband Antenna Array Based on Polymer Technology for Brain Stroke Diagnosis," *IEEE Trans. Biomed. Circuits Syst.*, vol. 13, no. 1, pp. 124-134, Feb. 2019.

[13] T. Carey et al., "Fully inkjet-printed two-dimensional material field-effect heterojunctions for wearable and textile electronics," *Nat. Commun.*, vol. 8, Oct 31 2017.

[14] S. Genovesi, F. Costa, F. Fanciulli and A. Monorchio, "Wearable Inkjet-Printed Wideband Antenna by Using Miniaturized AMC for Sub-GHz Applications," *IEEE Antennas Wirel. Propag. Lett.*, vol. 15, pp. 1927-1930, 2016.

[15] M. M. Rahman, M. A. Nayeem, S. Nahid, S. R. Bin Alvee, R. Rashidul Hasan and M. A. Rahman, "On-Body Humidity Sensing Antenna with Polyimide for BAN Applications over 5G Networks," *2020 IEEE International IOT, Electronics and Mechatronics Conference (IEMTRONICS)*, Vancouver, BC, Canada, 2020, pp. 1-7.

[16] A. S. M. Sayem, R. B. V. B. Simorangkir, K. P. Esselle, R. M. Hashmi and H. Liu, "A Method to Develop Flexible Robust Optically Transparent Unidirectional Antennas Utilizing Pure Water, PDMS, and Transparent Conductive Mesh," *IEEE Trans. Antennas Propag.*, vol. 68, no. 10, pp. 6943-6952, Oct. 2020.

[17] R. B. V. B. Simorangkir, A. Kiourti and K. P. Esselle, "UWB Wearable Antenna With a Full Ground Plane Based on PDMS-Embedded Conductive Fabric," *IEEE Antennas Wirel. Propag. Lett.*, vol. 17, no. 3, pp. 493-496, March 2018.

[18] R. Quarfoth, Y. Zhou and D. Sievenpiper, "Flexible Patch Antennas Using Patterned Metal Sheets on Silicone," *IEEE Antennas Wirel. Propag. Lett.*, vol. 14, pp. 1354-1357, 2015.
[19] B. Almohammed, et al. "Electro-Textile Wearable Antennas in Wireless Body Area Networks: Materials, Antenna Design, Manufacturing Techniques, and Human Body Consideration—a Review," *Textile Research Journal*, vol. 0, pp. 1-18, July 2020.
[20] J. Xiong, X. Lin, Y. Yu, M. Tang, S. Xiao and B. Wang, "Novel Flexible Dual-Frequency Broadside Radiating Rectangular Patch Antennas Based on Complementary Planar ENZ or MNZ Metamaterials," *IEEE Trans. Antennas Propag.*, vol. 60, no. 8, pp. 3958-3961, Aug. 2012.
[21] J. Park, Y. Ryu, J. Lee and J. Lee, "Epsilon Negative Zeroth-Order Resonator Antenna," *IEEE Trans. Antennas Propag.*, vol. 55, no. 12, pp. 3710-3712, Dec. 2007.
[22] J. Hao et al., "Textile split ring resonator antenna integrated by embroidery," *Electr. Lett.*, vol. 55, no. 9, pp. 508-509, May 2 2019.
[23] S. Yan, P. J. Soh and G. A. E. Vandenbosch, "Compact All-Textile Dual-Band Antenna Loaded With Metamaterial-Inspired Structure," *IEEE Antennas Wirel. Propag. Lett.*, vol. 14, pp. 1486-1489, 2015.
[24] J. Park, Y. Ryu, J. Lee and J. Lee, "Epsilon Negative Zeroth-Order Resonator Antenna," *IEEE Trans. Antennas Propag.*, vol. 55, no. 12, pp. 3710-3712, Dec. 2007.
[25] P. Y. Chen and A. Alù, "Sub-Wavelength Elliptical Patch Antenna Loaded With μ-Negative Metamaterials," *IEEE Trans. Antennas Propag.*, vol. 58, no. 9, pp. 2909-2919, Sept. 2010.
[26] P. Y. Chen and A. Alu, "Dual-Mode Miniaturized Elliptical Patch Antenna With μ-Negative Metamaterials," *IEEE Antennas Wirel. Propag. Lett.*, vol. 9, pp. 351-354, 2010.
[27] S. M. Saeed, C. A. Balanis, C. R. Birtcher, A. C. Durgun and H. N. Shaman, "Wearable Flexible Reconfigurable Antenna Integrated With Artificial Magnetic Conductor," *IEEE Antennas Wirel. Propag. Lett.*, vol. 16, pp. 2396-2399, 2017.
[28] M. Saleem and X. L. Li, "Low Scattering Microstrip Antenna Based on Broadband Artificial Magnetic Conductor Structure," *Materials*, vol. 13, no. 3, Feb 1 2020.
[29] B. S. Cook and A. Shamim, "Utilizing Wideband AMC Structures for High-Gain Inkjet-Printed Antennas on Lossy Paper Substrate," *IEEE Antennas Wirel. Propag. Lett.*, vol. 12, pp. 76-79, 2013.
[30] H. R. Raad, A. I. Abbosh, H. M. Al-Rizzo and D. G. Rucker, "Flexible and Compact AMC Based Antenna for Telemedicine Applications," *IEEE Trans. Antennas Propag.*, vol. 61, no. 2, pp. 524-531, Feb. 2013.
[31] A. Y. I. Ashyap et al., "Compact and Low-Profile Textile EBG-Based Antenna for Wearable Medical Applications," *IEEE Antennas Wirel. Propag. Lett.*, vol. 16, pp. 2550-2553, 2017.
[32] B. S. Abirami and E. F. Sundarsingh, "EBG-Backed Flexible Printed Yagi–Uda Antenna for On-Body Communication," *IEEE Trans. Antennas Propag.*, vol. 65, no. 7, pp. 3762-3765, July 2017.
[33] Y. Chen and T. Ku, "A Low-Profile Wearable Antenna Using a Miniature High Impedance Surface for Smartwatch Applications," *IEEE Antennas Wirel. Propag. Lett.*, vol. 15, pp. 1144-1147, 2016.
[34] S. Zhu and R. Langley, "Dual-Band Wearable Antennas over EBG Substrate," *Electr. Lett.*, vol. 43, no. 3, pp. 141-142, 1 Feb. 2007.
[35] S. Zhu and R. Langley, "Dual-Band Wearable Textile Antenna on an EBG Substrate," *IEEE Trans. Antennas Propag.*, vol. 57, no. 4, pp. 926-935, April 2009.
[36] Q.Bai and R. Langley, "Crumpled integrated AMC antenna," *Electr. Lett.*, vol. 45, no. 13, pp. 662 -663, 18 June 2009.
[37] S.Velan et al., "Dual-Band EBG Integrated Monopole Antenna Deploying Fractal Geometry for Wearable Applications," *IEEE Antennas Wirel. Propag. Lett.*, vol. 14, pp. 249-252, 2015.
[38] R. Joshi et al., "Dual-Band, Dual-Sense Textile Antenna With AMC Backing for Localization Using GPS and WBAN/WLAN," *IEEE Access*, vol. 8, pp. 89468-89478, 2020.
[39] S. Yan, P. J. Soh and G. A. E. Vandenbosch, "Low-Profile Dual-Band Textile Antenna With Artificial Magnetic Conductor Plane," *IEEE Trans. Antennas Propag.*, vol. 62, no. 12, pp. 6487-6490, Dec. 2014.
[40] T. Yue, Z. H. Jiang and D. H. Werner, "A Compact Metasurface-Enabled Dual-Band Dual-Circularly Polarized Antenna Loaded with Complementary Split Ring Resonators," *IEEE Trans. Antennas Propag.*, vol. 67, no. 2, pp. 794-803, Feb. 2019.
[41] W. E. I. Liu, Z. N. Chen and X. Qing, "Broadband Low-Profile L-Probe Fed Metasurface Antenna With TM Leaky Wave and TE Surface Wave Resonances," *IEEE Trans. Antennas Propag.*, vol. 68, no. 3, pp. 1348-1355, March 2020.
[42] W. Liu, Z. N. Chen and X. Qing, "Metamaterial-Based Low-Profile Broadband Mushroom Antenna," *IEEE Trans. Antennas Propag.*, vol. 62, no. 3, pp. 1165-1172, March 2014.
[43] K. Zhang, G. A. E. Vandenbosch and S. Yan, "A Novel Design Approach for Compact Wearable Antennas Based on Metasurfaces," *IEEE Trans. Biomed. Circuits Syst.*, vol. 14, no. 4, pp. 918-927, Aug. 2020.
[44] S. Yan, K. Zhang and P. J. Soh, "A Wideband Wearable Antenna Based on Metasurface," *2020 IEEE International RF and Microwave Conference (RFM)*, Kuala Lumpur, Malaysia, 2020.
[45] K. Zhang, A. Zhang and S. Yan, "A Compact Antenna Based on Metasurface for WLAN Band," *2019 International Symposium on Antennas and Propagation (ISAP)*, Xi'an, China, pp. 1-3, 2019.
[46] C. Caloz and T. Itoh, Electromagnetic Metamaterials: Transmission Line Theory and Microwave Applications. Hoboken, NJ, USA: Wiley, 2005.
[47] A. Sanada, C. Caloz and T. Itoh, "Characteristics of the composite right/left-handed transmission lines," *IEEE Microw. Wireless Compon. Lett.,* vol. 14, no. 2, pp. 68-70, Feb. 2004.
[48] A. Sanada, C. Caloz and T. Itoh, "Planar distributed structures with negative refractive index," *IEEE Trans. Microwave Theory Tech.*, vol. 52, no. 4, pp. 1252-1263, April 2004.
[49] P. Chen and A. Alù, "Terahertz Metamaterial Devices Based on Graphene Nanostructures," *IEEE Trans. THz Sci. Technol.,* vol. 3, no. 6, pp. 748-756, Nov. 2013.
[50] Y. R. Padooru, A. B. Yakovlev, P. Y. Chen, and A. Alu, "Analytical modeling of conformal mantle cloaks for cylindrical objects using sub-wavelength printed and slotted arrays," *J. Appl. Phys.*, vol. 112, no. 7, Oct 1 2012.
[51] Y. R. Padooru, A. B. Yakovlev, P. Y. Chen, and A. Alu, "Line-source excitation of realistic conformal metasurface cloaks," *J. Appl. Phys.,* vol. 112, no. 10, Nov 15 2012.
[52] W. Sun, Y. Li, Z. Zhang and Z. Feng, "Broadband and Low-Profile Microstrip Antenna Using Strip-Slot Hybrid Structure," *IEEE Antennas Wirel. Propag. Lett.*, vol. 16, pp. 3118-3121, 2017.
[53] Y. M. Pan, P. F. Hu, X. Y. Zhang and S. Y. Zheng, "A Low-Profile High-Gain and Wideband Filtering Antenna With Metasurface," *IEEE Trans. Antennas Propag.*, vol. 64, no. 5, pp. 2010-2016, May 2016.
[54] M. Shahpari and D. V. Thiel, "Fundamental Limitations for Antenna Radiation Efficiency," *IEEE Trans. Antennas Propag.*, vol. 66, no. 8, pp. 3894-3901, Aug. 2018.
[55] P. J. Soh, G. Vandenbosch, F. H. Wee, A. van den Bosch, M. Martinez-Vazquez and D. Schreurs, "Specific Absorption Rate (SAR) Evaluation of Textile Antennas," *IEEE Antennas Propag. Mag.*, vol. 57, no. 2, pp. 229-240, April 2015.

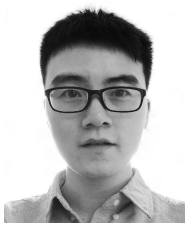

Kai Zhang received his bachelor's degree from Xi'an Shiyou University, Xi'an, China, in 2015, and master's degrees from Xidian University, Xi'an, in 2018. He is currently pursuing the Ph.D. degree with electronics science and technology, Xi'an Jiaotong University, Xi'an, China. His current research interests include metamaterials and metasurfaces, wearable devices and textile antennas.

Ping Jack Soh (S'10, M'14, SM'15) received the bachelor's and master's degrees from the Universiti Teknologi Malaysia, and the Ph.D. degree from KU Leuven, Belgium.

He is currently an Associate Professor in the Centre for Wireless Communications (CWC), University of Oulu, Finland. He started his career as a Test Engineer (2002–2004) and a Research and Development

Engineer (2005–2006). He then joined Universiti Malaysia Perlis (UniMAP), as a Lecturer, (2006–2009), before moving to KU Leuven, as a Research Assistant (2009–2013), a Postdoctoral Research Fellow (2013–2014), and since 2014, a Research Affiliate with the ESAT-WAVECORE Research Division. He went back to UniMAP as a Senior Lecturer (2014–2017) and an Associate Professor (2017–2021), before moving to Finland. Within UniMAP, he was formerly the Deputy Director of the Centre for Industrial Collaboration (2007–2009), the Deputy Dean of the university's Research Management and Innovation Center (RMIC) (2014–2017), and the Head of the Advanced Communication Engineering (ACE) Research Centre (2020). His research interests include antennas and related technologies; focused on their applications in wearables/body area communication; compact satellites; metasurfaces; 5G/6G communications; EM safety and absorption; and wireless techniques for healthcare.

Dr. Soh is a member of the IET and URSI. He was a recipient of the URSI Young Scientist Award in 2015, the IEEE MTT-S Graduate Fellowship for Medical Applications in 2013, and the IEEE AP-S Doctoral Research Award in 2012. He was also the Second Place Winner of the IEEE Presidents' Change the World Competition in 2013. He is a Chartered Engineer registered with the U.K. Engineering Council. He also volunteers in the IEEE MTT-S Education Committee. He is also an Associate Editor of the International Journal of Numerical Modelling: Electronic Networks, Devices and Fields (Wiley).

Sen Yan (M'17) received his bachelor's and master's degrees in information and communication engineering from Xi'an Jiaotong University (XJTU), Xi'an, China, in 2007 and 2010, respectively, and the Ph.D. degree in electrical engineering from Katholieke Universiteit Leuven (KU Leuven), Leuven, Belgium, in 2015. From 2015 to 2017, he was a Post-Doctoral Researcher with KU Leuven. In 2016, he joined EPFL, Lausanne, Switzerland, and the University of Texas at Austin, Austin, TX, USA, as a Visiting Researcher. Since 2017, he has been a Full Professor with XJTU.

Prof. Yan has authored or co-authored 75 international journal papers and 76 conference contributions. His current research interests include metamaterials and metasurfaces, wearable devices and textile antennas, reconfigurable antennas, antenna diversity, and biosensors. He was successful in achieving the Post-Doctoral Fellowship from KU Leuven and FWO in 2015 and 2016, respectively. In 2017, he received the ''Young Talent Support Plan'' from XJTU. In 2019, he received the "Young Scientist Award" of the International Union of Radio Science (URSI).